A&A 529, A116 (2011)
DOI: 10.1051/0004-6361/201016352

Astronomy & Astrophysics

XMM-Newton observations of the X-ray soft polar QS Telescopii⋆

I. Traulsen[1,2], K. Reinsch[1], A. D. Schwope[2], V. Burwitz[3], S. Dreizler[1], R. Schwarz[2], and F. M. Walter[4]

[1] Institut für Astrophysik, Georg-August-Universität Göttingen, Friedrich-Hund-Platz 1, 37077 Göttingen, Germany
e-mail: traulsen@astro.physik.uni-goettingen.de
[2] Astrophysikalisches Institut Potsdam, An der Sternwarte 16, 14482 Potsdam, Germany
[3] Max-Planck-Institut für Extraterrestrische Physik, PO Box 1312, 85741 Garching, Germany
[4] Department of Physics and Astronomy, Stony Brook University, Stony Brook, NY 11794-3800, USA

Received 17 December 2010 / Accepted 15 March 2011

ABSTRACT

Context. On the basis of *XMM-Newton* observations, we investigate the energy balance of selected magnetic cataclysmic variables, which have shown an extreme soft-to-hard X-ray flux ratio in the ROSAT All-Sky Survey.
Aims. We intend to establish the X-ray properties of the system components, their flux contributions, and the accretion geometry of the X-ray soft polar QS Tel. In the context of high-resolution X-ray analyses of magnetic cataclysmic variables, this study will contribute to better understanding the accretion processes on magnetic white dwarfs.
Methods. During an intermediate high state of accretion of QS Tel, we have obtained 20 ks of *XMM-Newton* data, corresponding to more than two orbital periods, accompanied by simultaneous optical photometry and phase-resolved spectroscopy. We analyze the multi-wavelength spectra and light curves and compare them to former high- and low-state observations.
Results. Soft emission at energies below 2 keV dominates the X-ray light curves. The complex double-peaked maxima are disrupted by a sharp dip in the very soft energy range (0.1−0.5 keV), where the count rate abruptly drops to zero. The EPIC spectra are described by a minimally absorbed black body at 20 eV and two partially absorbed MEKAL plasma models with temperatures around 0.2 and 3 keV. The black-body-like component arises from one mainly active, soft X-ray bright accretion region nearly facing the mass donor. Parts of the plasma emission might be attributed to the second, virtually inactive pole. High soft-to-hard X-ray flux ratios and hardness ratios demonstrate that the high-energy emission of QS Tel is substantially dominated by its X-ray soft component.

Key words. novae, cataclysmic variables – stars: fundamental parameters – stars: individual: QS Telescopii – X-rays: binaries – accretion, accretion disks

1. Introduction

QS Tel belongs to the group of AM Her-type cataclysmic variables, in which the field strength of the white-dwarf primary is high enough to prevent the formation of an accretion disk. It has been discovered in the ROSAT All-Sky Survey, independently in the soft X-ray regime by Beuermann & Thomas (1993) and in the EUV by Buckley et al. (1993). Survey and pointed ROSAT observations revealed a distinct soft X-ray flux component. With an orbital period of 2.33 h, it is one of the few systems that settle in the period gap of cataclysmic variables. The magnetic field strength M = 50−80 MG of the white dwarf in QS Tel ranges among the highest values measured in AM Her-type systems. Undergoing frequent changes between high and low states and occasionally switching between one-pole accretion (e.g. Buckley et al. 1993) and two-pole accretion (e.g. Rosen et al. 1996), QS Tel exhibits a variety of accretion behaviors and has been subject to various multi-wavelength studies.

We are obtaining *XMM-Newton* data of soft X-ray selected polars which have not been subject to high-resolution X-ray observations before, and investigate the system properties and a potential dominance of the soft over the hard X-ray flux ("soft X-ray excess"). This paper on the soft polar QS Tel is the second in a series dealing with the results of our campaign. In Sect. 2, we present our observational X-ray and optical data. Section 3 summarizes the results of the light-curve and Sect. 4 of the spectral analyses, respectively. Finally, we discuss the implications on accretion state and accretion geometry in Sect. 5.

2. Observations and data reduction

QS Tel was observed with *XMM-Newton* on September 30, 2006 for 20 ks (archived under observation ID 0404710401). The EPIC/pn detector was operated in large window mode with the medium filter, EPIC/MOS2 in small window mode with the thin filter. EPIC/MOS1 suffered from a full scientific buffer in timing mode and collected too little signal. With the optical monitor, we performed ultraviolet fast mode photometry in the 2050−2450 Å band using the *UVM2* filter. We employ SAS v8.0 standard tasks for the data reduction and apply an effective area correction as described by Traulsen et al. (2010) for the EPIC spectra of AI Tri. For the EPIC instruments, we choose a circular source region with a radius of 25 arcsec. The EPIC/pn background can be taken from the same chip as the source. Due to gaps in the detector plane close to the source, we determine the EPIC/MOS2 background from a source-free region on an outer CCD. The net peak count rates of 2.2 ± 0.6 cts s^{-1} for EPIC/pn and 0.70 ± 0.26 cts s^{-1} for EPIC/MOS2, respectively, are about a factor of

⋆ Based on observations obtained with *XMM-Newton*, an ESA science mission with instruments and contributions directly funded by ESA Member States and NASA.

eight lower than expected during high states from the ROSAT All-Sky Survey (Voges et al. 1999; Schwope et al. 1995). This means that QS Tel was in an intermediate high state of accretion at the epoch of our observations.

Contemporary optical observations have been performed at the CTIO observatory of the SMARTS consortium on October 1, 2006. *B*-band photometry with the ANDICAM at the 1.3 m telescope covers 85% of an orbital period with a cycle time of 100 s (73 data points). Taken under poor weather conditions, the data are non-photometric with a low signal-to-noise. Light curves are derived by differential photometry and calibrated as described by Gerke et al. (2006). 33 phase-resolved optical spectra in the 3500−5300 Å range were obtained with the R-C spectrograph at the 1.5 m telescope during about 80% of an orbital cycle. They show a spectral resolution of 4.5 Å in *FWHM* and a time resolution of 214 s. About half of the spectra are affected by clouds and cannot be used for a quantitative spectral analysis.

All times have been corrected to the barycenter of the solar system using the JPL ephemeris (Standish 1998) and converted to terrestrial time.

3. Optical data and multi-wavelength light curves

3.1. Constraining the binary ephemeris

The optical light curve profiles of QS Tel exhibit a changing morphology (see e.g. Rosen et al. 2001) and lack a definite recurring feature that could be used to establish photometric ephemeris. Schwope et al. (1995) derive a linear spectroscopic ephemeris for the broad and for the narrow emission line components, defining $\varphi_{\rm NEL} = 0.0$ at the blue-to-red zero crossing (inferior conjunction of the secondary). In order to verify the accuracy of their ephemeris, we investigate new optical phase-resolved spectra of QS Tel ($\Delta\varphi = 0.025$). The radial velocity curves show a large velocity amplitude $K > 300$ km s^{-1} and an asymmetric, non-sinusoidal shape, as described by Buckley et al. (1993), Schwope et al. (1995), and Rosen et al. (1996). Since our radial-velocity measurements are consistent with their data to better than $\Delta\varphi \sim 0.06$, we consider the ephemeris given by Schwope et al. (1995) to be still valid for our 2006 September 30 observations and refer to the phasing of the narrow emission line component (their Eq. (2)) throughout the analysis. We find no clear evidence of an orbital period change.

3.2. X-ray light curves

Figures 1a−d show the EPIC/pn photometric data folded on the orbital period. The soft X-ray emission at energies between 0.1 and 0.5 keV is characterized by high flaring variability and a distinct bright/faint behavior. At energies between 0.5 and 2.0 keV, the count rate is lower, and the bright phases are less pronounced than in the softest energy range. The flux at energies above 2 keV is very low, but non-zero during almost the complete orbital cycle. In all energy bands, the bright phases last about 40% of the binary revolution. The maxima are two-fold disrupted by dips in the flux: a broader, shallow dip lasting $\Delta\varphi \sim 0.08$ occurs around orbital phase 0.9. A sharp dip at $\varphi \sim 0.07$ ($\Delta\varphi < 0.02$) appears to be restricted to the very soft X-ray component at energies between 0.1 and 0.5 keV. During this short dip phase, the count rate nearly drops to zero (cf. Fig. 2), and the hardness ratio increases. We discuss the possible origin of the dips in Sect. 5.1.3.

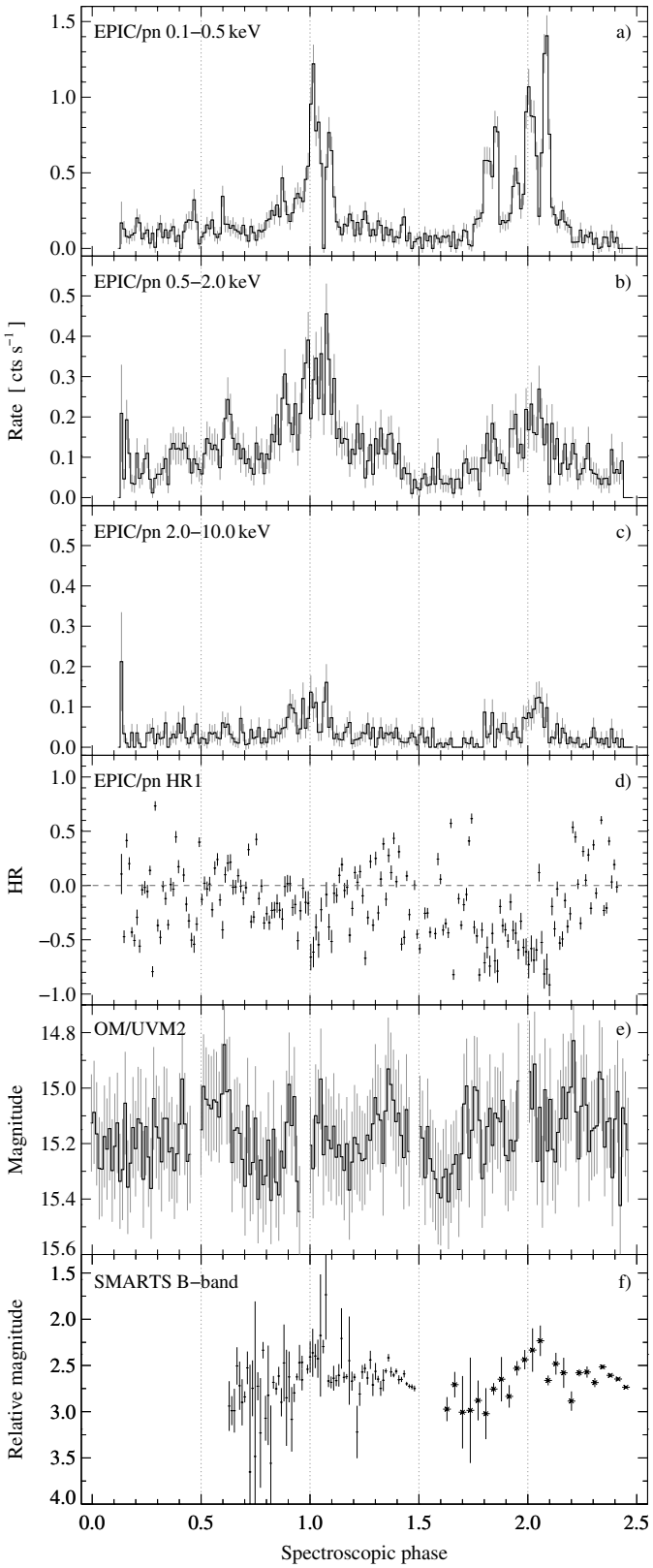

Fig. 1. Multi-wavelength light curves of QS Tel, folded on the orbital period. Phase zero corresponds to the inferior conjunction of the secondary star. **a)**−**c)** EPIC/pn light curves. **d)** Hardness ratio HR1 = (H−S)/(H+S) between the counts in the 0.1−0.5 keV and in the 0.5−2.0 keV ranges. **e)** Ultraviolet OM light curve in the 2050−2450 Å band. All *XMM-Newton* data are shown in time bins of 100 s. **f)** Optical SMARTS light curve, obtained simultaneously to the *XMM-Newton* observation. The data have been plotted twice, to the left with the original cycle time of 100 s, to the right rebinned into intervals of 300 s.

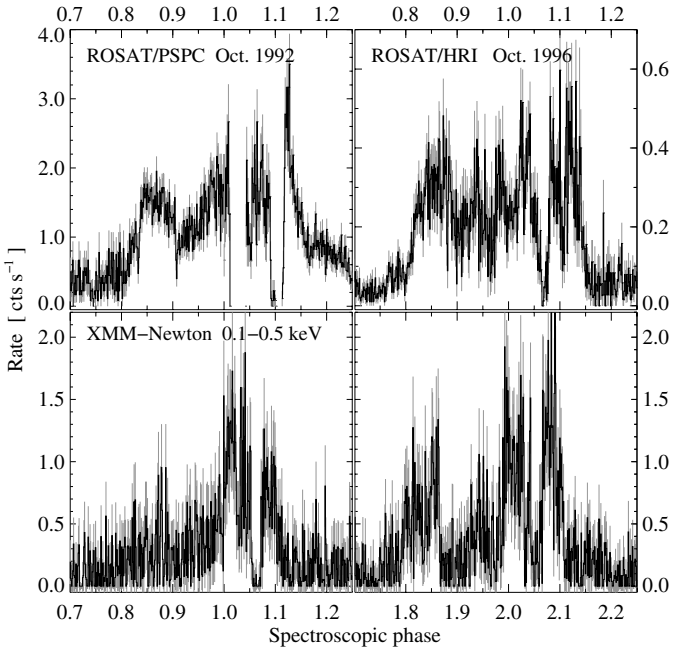

Fig. 2. Soft bright-phase light curves of QS Tel, binned into a time resolution of 10 s. *Upper panels*: archival ROSAT/PSPC and HRI data. *Lower panels*: EPIC/pn light curve in the 0.1–0.5 keV band.

3.3. B-band and ultraviolet light curves

The ultraviolet light curve at an effective wavelength of 2310 Å (Fig. 1e) has a small amplitude of about 0.2 mag and does not repeat itself during the two orbital cycles covered. The optical *B*-band light curve also shows little modulation with the orbital phase and resembles the *V*-band light curves during a low state of accretion obtained by Ferrario et al. (1994). Higher variability may be revealed after rebinning the optical data into intervals of 300 s (Fig. 1f). Former optical light curves are characterized by significantly stronger orbital modulations than our data, show various different light-curve shapes and a striking short- and long-term variability. We find no obvious analog to our *B*-band and UV light curves in the numerous CTIO and SAAO observations presented by Rosen et al. (1996, 2001), or in the ultraviolet HST/FOS continuum light curves of de Martino et al. (1998) and Rosen et al. (2001). Detailed descriptions of the different light curve profiles of QS Tel are given by Rosen et al. (1996, 2001), and an overview of its *B*-band magnitude long-term evolution since 2003 by Gerke et al. (2006).

4. X-ray spectroscopy

To derive the spectral parameters and the flux contribution of the system components and to gain information on the accretion geometry, we analyze the mean and the phase-resolved *XMM-Newton* spectra of QS Tel. We fit the EPIC/pn and MOS2 spectra simultaneously in XSPEC v12.5 (Arnaud 1996; Dorman et al. 2003), combining black-body and MEKAL plasma emission components and twofold absorption terms: TBNEW[1] to account for the galactic absorption, using the cross-sections of Verner & Ferland (1996) and Verner et al. (1996) and the abundances of Wilms et al. (2000); and PCFABS, partially covering the plasma emission, to represent intrinsic photoelectric absorption. When determining MEKAL metal abundances, we refer to the results of Asplund et al. (2009) from three-dimensional hydrodynamic modeling.

[1] Most recent version of TBVARABS in XSPEC. See http://pulsar.sternwarte.uni-erlangen.de/wilms/research/tbabs/.

4.1. The orbital mean spectrum

QS Tel was in an intermediate high state of accretion during the *XMM-Newton* observation. The spectral fits, thus, result in relatively low black-body and plasma temperatures, from which a rich metallic line spectrum arises. Our simplest fit consists of one black-body and one MEKAL component and the interstellar and intrinsic absorption terms. It implies a modest $\chi^2_{\rm red} = 1.22$ at 182 degrees of freedom. The soft X-ray range (0.1–0.4 keV) is well described by the single black body at $kT_{\rm bb} = 21.1^{+3.5}_{-3.0}$ eV and barely affected by interstellar absorption ($N_{\rm H,ISM} = 3.3^{+5.9}_{-2.0} \times 10^{19}$ cm^{-2}). These results are in perfect agreement with the fit of Rosen et al. (1996) to a ROSAT/PSPC spectrum, also taken during an intermediate high state, which yields $kT_{\rm bb} = 20.5^{+1.5}_{-1.8}$ eV and $N_{\rm H} = 3.3^{+1.0}_{-0.7} \times 10^{19}$ cm^{-2}. The X-ray spectrum at energies above 0.4–0.5 keV is approximated by a MEKAL spectrum at a mean temperature of $kT_{\rm MEKAL} = 2.2^{+0.4}_{-0.3}$ keV, comparable to the temperature of an only slightly absorbed bremsstrahlung component $kT_{\rm br} = 4.4 \pm 0.9$ keV that Rosen et al. (2001) derive from an ASCA spectrum of QS Tel. Additional plasma components decrease the $\chi^2_{\rm red}$ of our fits, indicating the need for multi-temperature models, but result in large error bars of the MEKAL temperatures and fluxes.

We, therefore, test different temperature structures, using three alternative plasma models in XSPEC: CEMEKL, MKCFLOW, and the accretion-flow model spectra that have been presented by Traulsen et al. (2010) and are based on the calculations of Fischer & Beuermann (2001). They fit the hard component slightly better than a single MEKAL. The effect is mainly visible from the Ca 4.6 keV and the Fe 6.7 keV lines. Anyhow, all the fits under-estimate the prominent calcium emission around 4.6 keV. The element abundances resulting from the different fits deviate from each other by a factor of up to two, with a clear trend to subsolar values. The strong correlation between plasma temperature, mass accretion rate, and element abundance in the models cause the large systematic uncertainties when determining the chemical composition of the accretion stream. None of these approaches results in a significantly better $\chi^2_{\rm red}$ than two-MEKAL fits.

The best fits are given by two multi-component models, each comprising two MEKAL components with independent temperatures and identical element abundances (see Table 1 and Fig. 3). In the first model, we use one common absorption term for both the MEKAL components, assuming that they arise from the same emission region (TBNEW(BBODY + PCFABS(MEKAL+MEKAL))). It yields MEKAL temperatures of $kT_{\rm MEKAL,low} = 0.21^{+0.03}_{-0.03}$ keV and $kT_{\rm MEKAL,high} = 2.8^{+0.8}_{-0.4}$ keV at a mean element abundance of $0.9^{+0.4}_{-0.2}$ times the solar ($\chi^2_{\rm red} = 1.06$ at 180 d.o.f.).

In the second model, we use an individual absorption term for each MEKAL component, assuming that they arise from different emission regions (TBNEW(BBODY + PCFABS(MEKAL) + PCFABS(MEKAL))). It infers the lowest $\chi^2_{\rm red} = 1.00$ at 178 d.o.f. The low-temperature MEKAL component at $kT_{\rm MEKAL,low} = 0.19^{+0.02}_{-0.03}$ keV is accompanied by intrinsic absorption of $N_{\rm H,intr} = 1.6^{+3.7}_{-3.6} \times 10^{22}$ cm^{-2} with a high covering fraction close to one. The high-temperature component results in $kT_{\rm MEKAL,high} = 3.3^{+0.9}_{-0.6}$ keV and $N_{\rm H,intr} = 6.1^{+4.1}_{-2.5} \times 10^{22}$ cm^{-2}, which is partially covered by a factor of $0.5^{+0.1}_{-0.2}$. The absorption and temperature of the low-

Table 1. Best-fit parameters of the models with one and two MEKAL plasma components, respectively, for the EPIC spectra of QS Tel (orbital mean).

χ^2_{red}	$N_{H,ISM}$ [10^{19} cm^{-2}]	kT_{bb} [eV]	$N_{H,intr}$ [10^{22} cm^{-2}]	cover.	kT_{MEKAL} [keV]	kT_{MEKAL} [keV]	abund.	F_{bol}(BBODY) [erg cm^{-2} s^{-1}]	F_{bol}(MEKAL) [erg cm^{-2} s^{-1}]
TBNEW(BBODY+PCFABS(MEKAL))									
1.22	$3.3^{+5.9}_{-2.9}$	$21.1^{+3.5}_{-3.0}$	$16.1^{+7.7}_{-4.5}$	$0.74^{+0.07}_{-0.11}$		$2.2^{+0.4}_{-0.3}$	$0.4^{+0.2}_{-0.1}$	$1.2^{+7.3}_{-0.8} \times 10^{-11}$	$1.7^{+0.5}_{-0.5} \times 10^{-12}$
TBNEW(BBODY+PCFABS(MEKAL+MEKAL))									
1.06	$9.3^{+14.7}_{-7.5}$	$19.2^{+5.4}_{-3.5}$	$11.8^{+7.4}_{-3.8}$	$0.60^{+0.13}_{-0.23}$	$0.21^{+0.03}_{-0.03}$	$2.8^{+0.8}_{-0.4}$	$0.9^{+0.4}_{-0.2}$	$3.8^{+16.7}_{-3.3} \times 10^{-11}$	$1.3^{+0.2}_{-0.4} \times 10^{-12}$
TBNEW(BBODY+PCFABS(MEKAL)+PCFABS(MEKAL))									
1.00	$5.1^{+12.3}_{-4.2}$	$20.6^{+4.0}_{-4.0}$	$1.6^{+0.4}_{-0.4}$	$0.99^{+0.01}_{-0.01}$	$0.19^{+0.02}_{-0.03}$				$(2.7^{+0.4}_{-0.4} \times 10^{-11})^*$
			$6.1^{+4.1}_{-2.5}$	$0.53^{+0.14}_{-0.21}$		$3.3^{+0.9}_{-0.6}$	$1.2^{+0.6}_{-0.4}$	$1.6^{+0.2}_{-0.2} \times 10^{-11}$	$7.6^{+0.4}_{-0.4} \times 10^{-13}$

Notes. Fluxes have been determined via CFLUX within XSPEC. (*) The integrated flux of the low-temperature MEKAL component in this fit is highly sensitive even to small changes of temperature, abundance, and absorption, and should, therefore, be interpreted very carefully.

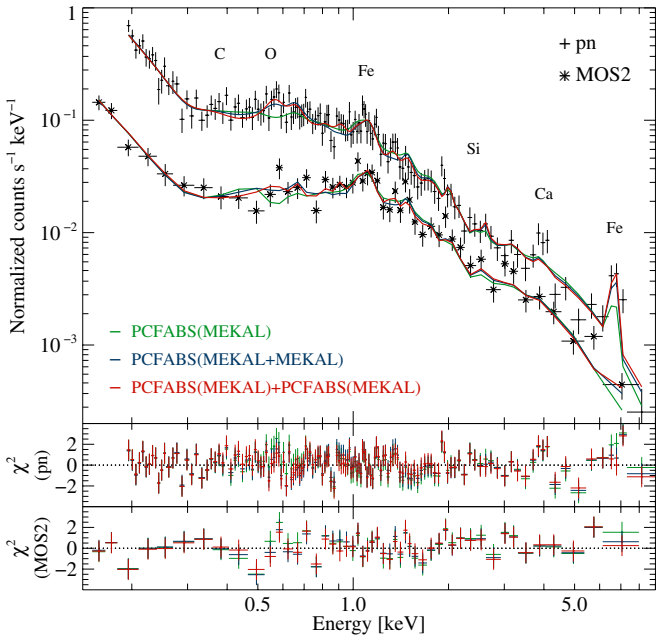

Fig. 3. EPIC/pn and MOS2 spectra of QS Tel and the XSPEC fits listed in Table 1. The models consist of a single black-body plus one and two partially absorbed MEKAL components, respectively. Spectral bins comprise a minimum of 20 counts.

energy black-body component agree with the result of the PCFABS(MEKAL+MEKAL) fit within the confidence range.

4.2. The X-ray bright and faint phases

The X-ray bright phases, defined by the on-off-behavior of the light curves in the softest energy range, cover the phase interval $\varphi = 0.7-1.1$. We extract one mean bright- and one mean faint-phase spectrum for each EPIC instrument from the two orbital cycles covered and fit them with the one- and two-MEKAL spectra as described in Sect. 4.1. Due to the smaller number of counts collected for the phase-resolved spectra, the uncertainties of the fit parameters are larger, in particular of the interstellar absorption term and the upper MEKAL temperature. Within these error bars, the resulting temperatures, abundances, and absorption terms can be considered as identical with the orbital means given in Table 1 and, thus, as constant over the orbital cycle. In particular, we see no significant variation of the intrinsic absorption terms with the phase. The fluxes that we derive for the individual model components, though, are clearly phase-dependent and further discussed in Sect. 5.2.

5. Discussion

5.1. Accretion geometry

The most prominent features in the multi-wavelength light curves and the phase-resolved spectra can provide information on the accretion geometry of the system, useful for interpreting the spectral and flux components and for attributing them to the different emission regions. Former optical, UV, and soft X-ray observations have shown that QS Tel changes between intervals of one-pole and two-pole accretion (Buckley et al. 1993; Schwope et al. 1995; Rosen et al. 1996, 2001). Schwope et al. (1995) identify the two accretion poles via two sets of cyclotron lines in the optical spectra. They suggest that one accretion pole with $B_1 \sim 47$ MG, which is located near the connecting line to the secondary, mainly emits in the soft X-ray regime, and that a second accretion pole with $B_2 \sim 70-80$ MG is optically bright. This also explains offsets in time between optically bright and EUV bright states as reported by Rosen et al. (2001). Romero-Colmenero et al. (2004) confirm the existence of two accretion poles by high-state polarimetric observations. All the ROSAT soft X-ray (Schwope et al. 1995; Rosen et al. 1996, 2001) and several EUV light curves (Buckley et al. 1993; Rosen et al. 2001) are characterized by one pronounced maximum per orbital cycle. During various EUVE observations by Rosen et al. (1996, 2001), the light curves were double-peaked. These two maxima may indicate accretion onto the two, independently fed poles.

Our soft X-ray light curves show the single maximum that can be explained by the orbital revolution of the main accretion region and are similar to the former ROSAT light curves. The detection of hard X-ray emission during the complete orbital cycle allows for two possible explanations of its nature: the main, soft X-ray bright accretion region is extended and undergoes a partial self-eclipse, or a significant fraction of the hard X-ray flux on the order of 50% arises from the second, optically bright accretion region. We discuss these scenarios and potential photometric and spectroscopic signs of them in the following two sections.

5.1.1. A partially self-eclipsing main accretion region

If the complete X-ray flux arises from the main pole, which almost faces the secondary, the faint-phase emission can be assigned to the uneclipsed outer parts of the accretion re-

gion. The accretion regions on the white-dwarf primaries in polars can show asymmetric and extended shapes, as investigated in detail for instance by Wickramasinghe et al. (1991) and Sirk & Howell (1998). Partial self-eclipses of such an extended accretion region have also been suggested by Beuermann et al. (1987) for EF Eri on the basis of Einstein light curves and by Schwope et al. (2000) for QQ Vul on the basis of polarimetric data. The soft X-ray emission of QS Tel is reduced by a factor of about ten during the faint phase, possibly by the self-eclipse of the inner part of the extended accretion region, while the MEKAL flux diminishes by a factor between two and three. The different MEKAL components in the spectral fits are completely attributed to the main accretion column in this picture, and the temperature structure of this column deviates from the ones of typical multi-temperature models in XSPEC (see Sect. 4.1). The similar MEKAL temperatures and partially covering absorption terms in the phase-resolved spectral models, then, continuously reflect the main accretion column.

5.1.2. Emission from the second accretion region

The (slightly variable) flux in the optical and ultraviolet wave bands can be attributed to the second, highly magnetic pole (Schwope et al. 1995), which, thus, accreted at a low level at the epoch of our observations. If this accretion pole also shapes the faint-phase light curves and spectra, a cooler black-body-like component might arise from the region around the second accretion column, with its flux maximum possibly shifted to lower energies. In this picture, the two MEKAL components have their origin in the two accretion poles, and the different absorption terms in the PCFABS(MEKAL) + PCFABS(MEKAL) models imply that the plasma emission is absorbed to different degrees around the two accretion columns. The spectral parameters (black-body luminosities, normalizations of the MKCFLOW models) indicate a mass accretion rate of approximately $\dot{M}_{\rm faint} \sim 10^{-12}\ M_\odot\ {\rm yr}^{-1}$ for the faint-phase and $\dot{M}_{\rm bright} \sim 10^{-10}\ M_\odot\ {\rm yr}^{-1}$ for the bright-phase fits. It is obvious that those models that rely on a typical temperature structure of a single accretion column cannot improve the fit quality compared to the two-MEKAL approaches, then (cf. Sect. 4.1). Another two-pole accreting polar in which the second accretion region is probably seen during the X-ray faint phase is BY Cam, one of the few asynchronous systems. Ramsay & Cropper (2002) assign the flaring bright light-curve intervals of BY Cam to a soft pole with "blobby" accretion, and the low, hard faint-phase flux to the second pole, whose soft emission is shifted into the ultraviolet range. The authors state two alternative reasons for the lower temperatures in the accretion region, which would cause the wavelength shift: the region is less effectively heated due to a low accretion rate, or the accreted material is spread over a rather extended accretion area.

For the interpretation of the spectral model components as emission of either one or two accretion pole(s), it may be instructive to evaluate the orbital modulation of their fluxes. Table 2 shows the phase-resolved bolometric fluxes that we derive from the two-MEKAL XSPEC models. For calculating the fluxes, temperatures and abundances are assumed to be constant over the binary cycle and set to their orbital means (Table 1). The flux of the low-temperature MEKAL component in the PCFABS(MEKAL) + PCFABS(MEKAL) fit stays essentially constant over the orbit, even though the large error bars have to be kept in mind. The high-temperature MEKAL flux changes clearly between bright and faint phase, but still to a lower degree than the black-body flux. This means: in case the two MEKALS can be attributed to two accretion columns, then the black body and the hotter MEKAL have their origin in the primary, soft X-ray bright region, and the cooler MEKAL in the second, less active one. A signature of the second accretion pole in the *XMM-Newton* data, hence, is possible, but not definite.

Table 2. Unabsorbed bolometric fluxes of the phase-resolved two-MEKAL model components, using constant temperatures and abundances (=orbital means) over the orbital cycle, and the corresponding black-body to MEKAL flux ratios.

$F_{\rm bol}$(BBODY)	$F_{\rm bol}$(MEKAL1)	$F_{\rm bol}$(MEKAL2)	$F_{\rm bb}/F_{\rm MEKAL}$	$F_{\rm bb}/F_{\rm MEKAL2}$
	[erg cm^{-2} s^{-1}]			
TBNEW(BBODY+PCFABS(MEKAL+MEKAL))				
Bright phase				
$1.2^{+1.6}_{-0.6} \times 10^{-10}$	$6.3^{+2.8}_{-2.5} \times 10^{-13}$	$1.8^{+0.4}_{-0.3} \times 10^{-12}$	47^{+67}_{-23}	
Faint phase				
$1.2^{+3.0}_{-0.9} \times 10^{-11}$	$2.1^{+1.3}_{-1.0} \times 10^{-13}$	$7.7^{+2.6}_{-1.8} \times 10^{-13}$	12^{+31}_{-9}	
TBNEW(BBODY+PCFABS(MEKAL)+PCFABS(MEKAL))				
Bright phase				
$5.3^{+6.4}_{-3.0} \times 10^{-11}$	$1.7^{+5.4}_{-1.2} \times 10^{-12}$	$1.5^{+0.4}_{-0.3} \times 10^{-12}$	17^{+20}_{-9}	35^{+43}_{-20}
Faint phase				
$3.2^{+4.3}_{-1.2} \times 10^{-12}$	$1.6^{+0.6}_{-1.0} \times 10^{-12}$	$5.8^{+1.4}_{-1.0} \times 10^{-13}$	$1.5^{+2.0}_{-0.6}$	6^{+7}_{-2}

5.1.3. The soft X-ray light-curve dips

Two dips have been described in the light curves of QS Tel at different wavelengths: a sharp dip recurs in the $\varphi = 0.0$–0.1 interval. It has been found by Rosen et al. (1996, 2001) and de Martino et al. (1998) in X-ray, EUV, and UV data. A broader trough around $\varphi \sim 0.9$ appears occasionally in the X-ray light curves and varies in depth. It is well pronounced for example in the ROSAT/PSPC light curve profile of Rosen et al. (1996).

Both dips can be identified in our X-ray light curves, which are similar to the ROSAT/PSPC and HRI light curves presented by Rosen et al. (1996, 2001). The broader trough around $\varphi \sim 0.9$ appears both in the 0.1–0.5 keV and in the 0.5–2.0 keV bands. Being variable and not strictly recurring, it could be an effect of random mass transfer variations, of structures in the accretion region, or an absorption feature, e.g. by an extended accretion column. Rosen et al. (1996, 2001) report a similar pre-dip structure in a ROSAT/WFC light curve and consider absorption as the most plausible explanation.

The narrow dip close to $\varphi \sim 0.07$ is mainly pronounced in the softest energy band and not seen in the optical light curves. Obviously a persisting feature, it also appears in the double-peaked EUVE light curves at similar orbital phase (Rosen et al. 1996, 2001). Minor shifts of its phasing within the $\varphi \sim 0.0$ and 0.1 interval are found both in the ROSAT/HRI, PSPC, and WFC and in the EUVE light curves (cf. Rosen et al. 1996, 2001, Fig. 2). The dip is generally explained by the accretion stream eclipsing the X-ray bright accretion region. The short ingress and egress times and the hardness-ratio peak during the dip phase fit in this picture, although it is difficult to be reconciled with the interpretation of $\varphi = 0.0$ as inferior conjunction of the secondary (cf. Sect. 3). Typically, the main accretion regions in polars are located at longitudes below 90° (Cropper 1988), which places a potential stream dip in the $\varphi = 0.75$–1.0 interval in this phase convention, less likely between $\varphi = 0.05$ and 0.10. A similar dip is seen in the EUVE light curves of UZ For around orbital phase 0.9 and could be due to stream absorption according to Warren et al. (1995). They point out that the influence of the

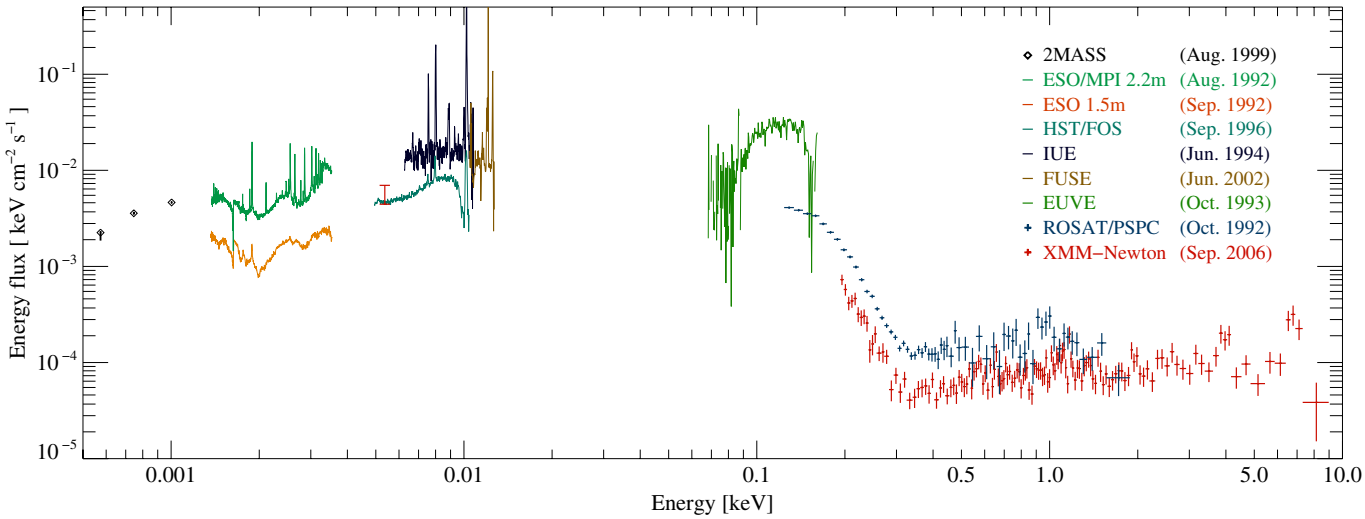

Fig. 4. Spectral energy distribution of QS Tel, including our *XMM-Newton* data and archival observations during different accretion states. The data point derived for the *XMM-Newton* optical monitor at 5.4 eV (2310 Å) is shown as orbital minimum and maximum.

mass accretion rate variations on the location of the threading region can explain why the phasing and the depth of the dips change between different orbital cycles. Similar flare-like activity characterizes our X-ray light curves (Sect. 5.2.2) and former ROSAT light curves of QS Tel (stated e.g. by Rosen et al. 1996), including the sharp dip. This, indeed, indicates $\dot{M}$ variations.

5.2. The soft X-ray excess

5.2.1. Bolometric flux ratios

As the excess of soft over hard X-ray emission in polars is expected to increase with the magnetic field strength (Beuermann & Schwope 1994; Ramsay et al. 1994), the high-field system QS Tel can serve as a test case. Both the X-ray light curves and the spectra of QS Tel indeed evince its very soft X-ray flux. The count rate decreases rapidly towards higher energies above 0.5 keV. From our fits to the *XMM-Newton* spectra, we derive bolometric flux ratios of the black-body to the plasma components that are significantly larger than one. This finding is consistent with the flux ratios estimated by Rosen et al. (1996) using EUVE and ROSAT data. Ramsay et al. (1994) and Ramsay & Cropper (2004), on the other hand, determine luminosity ratios in the range between 1.2 and 10.6 from ROSAT spectra of QS Tel, using a 30 keV-bremsstrahlung model for the high-energy component.

The actual values of the bolometric flux ratios during the X-ray bright phases depend on the spectral model and on the considered accretion scenario. Ratios of the total black-body to the total plasma flux correspond to the scenario of a partially eclipsed, extended main accretion region (Sect. 5.1.1). For the PCFABS(MEKAL+MEKAL) model, the integrated unabsorbed model fluxes, uncorrected for the viewing angle, give a ratio of $F_{\rm bb}/F_{\rm MEKAL} = 47^{+67}_{-23}$ during the bright phases. The analogous approach for PCFABS(MEKAL) + PCFABS(MEKAL) results in $F_{\rm bb}/F_{\rm MEKAL} = 17^{+20}_{-9}$, using the total flux of both MEKAL components. If the low-temperature MEKAL component is attributed to the second accretion region (scenario Sect. 5.1.2), we have to compare the black-body and the high-temperature MEKAL component in order to derive the flux ratio of the primary accretion pole: $F_{\rm bb}/F_{\rm MEKAL,high} = 35^{+43}_{-20}$. Thus, we can confirm a distinct soft X-ray excess of the primary accretion region in QS Tel, in which the black-body component has its origin.

Figure 4 compares the energy flux of our *XMM-Newton* and optical observations to archival multi-wavelength data. From our fits to the EPIC spectra, we derive a total integrated flux on the order of $F_{\rm bol} \sim 10^{-11}$ erg cm^{-2} s^{-1} and a bolometric model luminosity on the order of $L_{\rm bb} \sim 10^{31}(d/176\ {\rm pc})^2$ erg s^{-1}, using the distance determined by Ak et al. (2007). These results are two orders of magnitude lower than those determined for the EUVE high-state data by Rosen et al. (1996). The values that they derive from ROSAT spectra, also obtained during an intermediate high state of accretion, are similar to our *XMM-Newton* results. As a higher mass accretion rate is expected to affect the soft component mainly, our intermediate-state hardness and flux ratios can serve as lower limits for the high-state cases.

5.2.2. The soft X-ray light curves

The hardness ratios, positive over large parts of the orbital cycle, reflect the little spectral contribution of events at energies above 0.5 keV. A distinct soft X-ray excess is most probably connected to the "blobby" accretion scenario (Beuermann 2004), causing a flaring structure of the X-ray light curves. Despite the moderate count rate during the *XMM-Newton* pointing, individual flare events with a typical duration of 10−15 s appear in the soft X-ray light curves, mostly during the bright phases. These events can be assigned to separate filaments in the accretion stream permeating the white-dwarf atmosphere at a low rate. The patterns are comparable to the flares in the light curves of V1309 Ori (Schwarz et al. 2005), which show – at a considerably higher count rate – clear evidence of single accretion blobs.

The strong flickering appears to be present at all wavelengths from the optical down to soft X-rays (e.g. Rosen et al. 1996; de Martino et al. 1998; Rosen et al. 2001). Warren et al. (1993) find flare-like events during a low state of accretion, which they explain as the potential impact of accretion blobs at a low mass transfer rate or as magnetic flares. This short-time variability provides further evidence of clumpy accretion events, as typical of soft X-ray dominated systems.

6. Summary

At the epoch of our *XMM-Newton* observations, QS Tel was in an intermediate high state of accretion, where most accretion activity was concentrated on the primary, soft X-ray bright pole. The soft X-ray light curves are characterized by a distinct bright phase, lasting about 40% of the binary orbit. We identify the sharp dip in the soft X-ray light curve that has been seen in all previous ROSAT X-ray and various EUVE observations, and confirm that it is most likely due to an occultation of the soft X-ray emitting region by the accretion stream. The light curves in the hard X-ray, UV, and optical regime show little orbital modulation. The best fits to the X-ray spectra consist of one black-body and two absorbed plasma components. Whether these plasma components have their origin in different emission areas around the primary accretion pole or in independent accretion onto the two poles cannot be finally decided from our spectra. The modulation of the phase-resolved model fluxes indicates that the low-temperature plasma component might represent the second, optically bright accretion pole. The bolometric flux ratios of the soft (black-body) and the hard (MEKAL) components are strongly model dependent and in the range of 15 to about 120 during the bright phases. Together with the high short-term variability of the soft X-ray light curves, this finding establishes QS Tel as a distinctly soft X-ray dominated, "blobby" accreting system.

Acknowledgements. This research has been granted by DLR under project numbers 50 OR 0501 and 50 OR 0807. We have obtained the ROSAT/PSPC and HRI data from the High Energy Astrophysics Science Archive Research Center (HEASARC), provided by NASA's Goddard Space Flight Center, and the EUVE, FUSE, IUE, and HST spectra from the Multimission Archive at the Space Telescope Science Institute (MAST).

References

Ak, T., Bilir, S., Ak, S., & Retter, A. 2007, New Astron., 12, 446
Arnaud, K. A. 1996, in Astronomical Data Analysis Software and Systems V, ed. G. H. Jacoby, & J. Barnes, ASP Conf. Ser., 101, 17
Asplund, M., Grevesse, N., Sauval, A. J., & Scott, P. 2009, ARA&A, 47, 481
Beuermann, K. 2004, in Magnetic Cataclysmic Variables, ed. S. Vrielmann, & M. Cropper, IAU Colloq., 190, ASP Conf. Ser., 315, 187
Beuermann, K., & Schwope, A. D. 1994, in Interacting Binary Stars, ed. A. W. Shafter, ASP Conf. Ser., 56, 119
Beuermann, K., & Thomas, H.-C. 1993, Adv. Space Res., 13, 115
Beuermann, K., Stella, L., & Patterson, J. 1987, ApJ, 316, 360
Buckley, D. A. H., O'Donoghue, D., Hassall, B. J. M., et al. 1993, MNRAS, 262, 93
Cropper, M. 1988, MNRAS, 231, 597
de Martino, D., Mouchet, M., Rosen, S. R., et al. 1998, A&A, 329, 571
Dorman, B., Arnaud, K. A., & Gordon, C. A. 2003, in BAAS, 35, 641
Ferrario, L., Wickramasinghe, D. T., Bailey, J. A., & Buckley, D. A. H. 1994, MNRAS, 268, 128
Fischer, A., & Beuermann, K. 2001, A&A, 373, 211
Gerke, J. R., Howell, S. B., & Walter, F. M. 2006, PASP, 118, 678
Ramsay, G., & Cropper, M. 2002, MNRAS, 334, 805
Ramsay, G., & Cropper, M. 2004, MNRAS, 347, 497
Ramsay, G., Mason, K. O., Cropper, M., Watson, M. G., & Clayton, K. L. 1994, MNRAS, 270, 692
Romero-Colmenero, E., Potter, S. B., & Buckley, D. A. H. 2004, AN, 325, 214
Rosen, S. R., Mittaz, J. P. D., Buckley, D. A., et al. 1996, MNRAS, 280, 1121
Rosen, S. R., Rainger, J. F., Burleigh, M. R., et al. 2001, MNRAS, 322, 631
Schwarz, R., Reinsch, K., Beuermann, K., & Burwitz, V. 2005, A&A, 442, 271
Schwope, A. D., Thomas, H.-C., Beuermann, K., et al. 1995, A&A, 293, 764
Schwope, A. D., Catalán, M. S., Beuermann, K., et al. 2000, MNRAS, 313, 533
Sirk, M. M., & Howell, S. B. 1998, ApJ, 506, 824
Standish, E. M. 1998, JPL IOM, 312.F-98-048
Traulsen, I., Reinsch, K., Schwarz, R., et al. 2010, A&A, 516, A76
Verner, D. A., & Ferland, G. J. 1996, ApJS, 103, 467
Verner, D. A., Ferland, G. J., Korista, K. T., & Yakovlev, D. G. 1996, ApJ, 465, 487
Voges, W., Aschenbach, B., Boller, T., et al. 1999, A&A, 349, 389
Warren, J. K., Vallerga, J. V., Mauche, C. W., Mukai, K., & Siegmund, O. H. W. 1993, ApJ, 414, L69
Warren, J. K., Sirk, M. M., & Vallerga, J. V. 1995, ApJ, 445, 909
Wickramasinghe, D. T., Bailey, J., Meggitt, S. M. A., et al. 1991, MNRAS, 251, 28
Wilms, J., Allen, A., & McCray, R. 2000, ApJ, 542, 914